

Stainless steel-like FeCrNi nanostructures *via* electrodeposition into AAO templates using a mixed-solvent Cr(III)-based electrolyte

Enrico Bertero^{a,b,*}, Cristina V. Manzano^a, Gerhard Bürki^a, Laetitia Philippe^a

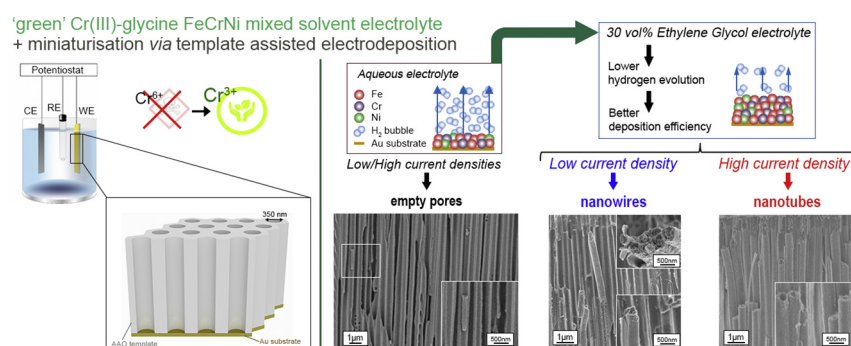
^a Empa - Swiss Federal Laboratories for Materials Science and Technology, Laboratory for Mechanics of Materials and Nanostructures, Feuerwerkerstrasse 39, 3602 Thun, Switzerland

^b Ecole Polytechnique Fédérale de Lausanne, Tribology and Interfacial Chemistry Group, Materials Institute Station 12 (SCI-STI-SM), 1015 Lausanne, Switzerland

HIGHLIGHTS

- Cr(III)-glycine complexation similar for aqueous and mixed solvent electrolytes
- Hydrogen evolution (HER) inhibited using mixed ethylene glycol (EG) electrolyte.
- Impurities incorporation in films decreases when using mixed solvent electrolyte.
- Electrodeposition of nanostructures is achieved only with EG mixed solution.
- FeCrNi nanotubes and nanowires formation depends on current density and HER.

GRAPHICAL ABSTRACT



ARTICLE INFO

Article history:

Received 16 October 2019

Received in revised form 19 December 2019

Accepted 7 February 2020

Available online 8 February 2020

Keywords:

FeCrNi alloy

Mixed-solvent electrolyte

Electrodeposition

Nanowires

Nanotubes

Anodic aluminium oxide

ABSTRACT

Electrodeposition of stainless steel-like materials such as FeCrNi alloy into micro- and nanotemplates provides a sustainable framework for creating biomedical-oriented micro- and nanocomponents with outstanding characteristics. While Cr(III)-based electrodeposition represents a 'green' alternative to toxic Cr(VI), its use is limited by Cr(III) aqueous chemistry which leads to the incorporation of impurities and the hydrogen evolution reaction (HER). These factors are responsible for low deposition efficiencies, brittleness and porosity. The current work sought to investigate the use of 'green' Cr(III)-glycine electrolyte to improve FeCrNi electrodeposition from Cr(III) precursors. Mixed-solvent electrolyte containing ethylene glycol (EG) was employed to reduce HER after-effects. FeCrNi mixed EG electrolytes were compared to their aqueous counterparts to observe differences in Cr(III)-glycine complexation, coatings' composition and current efficiency. The feasibility of this method for creating nanostructures was verified by template-assisted electrodeposition using anodic aluminium oxide (AAO) templates. This study established that mixed-solvent electrolytes are an effective strategy to improve Cr(III)-based plating of alloys into miniaturised moulds. For the first time, electrodeposited FeCrNi nanowires (NWs) and nanotubes (NTs) were achieved *via* the framework developed in this work. The possible mechanisms controlling the morphological variations in FeCrNi nanostructures were discussed in relation to the kinetic and growth models in single metal electroplating into nanotemplates.

© 2020 The Authors. Published by Elsevier Ltd. This is an open access article under the CC BY license (<http://creativecommons.org/licenses/by/4.0/>).

* Corresponding author at: Empa - Swiss Federal Laboratories for Materials Science and Technology, Laboratory for Mechanics of Materials and Nanostructures, Feuerwerkerstrasse 39, 3602 Thun, Switzerland.

E-mail addresses: enrico.bertero@empa.ch (E. Bertero), cristina.vicente@csic.es (C.V. Manzano), gerhard.buerki@empa.ch (G. Bürki), laetitia.philippe@empa.ch (L. Philippe).

1. Introduction

The interest in stainless steel (SS) is dictated by its good combination of properties as well as its relatively easy and low-cost fabrication processes. This makes it one of the most attractive and applied alloys worldwide. Additionally, stainless steel is a versatile material, as its final properties are tuneable through chemical composition modifications and applied treatments. This allows such alloys to find applications in many branches, specifically, austenitic stainless steels (e.g. AISI 304 and 316L) are extremely important in the bio-medical sector, due to their high corrosion and wear resistances, bio-compatibility, as well as good mechanical properties [1–3]. Recently, miniaturisation trends in the high-tech industry have pushed the development of advanced bio-medical applications and therefore, the investigation for viable fabrication techniques and appropriate materials. Among the available techniques (e.g. 3D printing, micro-powder injection), only electroplating into micro- and nanotemplates seems promising in terms of cost, performances, time and precision [4].

Electrodeposition has several advantages over other growth methods, as this technique is cost-effective, scalable and versatile, enabling to deposit inside high aspect ratio (AR) micro- (e.g. LIGA) and nano- (e.g. anodic aluminium oxide or polycarbonate) templates. Additionally, it allows a high degree of control over both crystallographic structure and morphology. This fabrication method has been used to successfully grow highly ordered NWs by plating inside anodic aluminium oxide (AAO) templates [5–8], to create such structures as ZnO NWs [9] or other metals and alloys containing mainly Co, Ni and Fe [10–19]. Research on electrodepositing metals and/or alloys into AAO membranes has been performed in the past, mainly for Ni, Fe, FeNi systems, as highly ordered nanostructures from these materials are sought when enhanced anisotropic magnetisation is of interest [10–13]. NWs of similar alloys have been achieved, typically by combining Co with Ni and/or Fe, e.g. CoNi [13], CoFe [16] and FeNiCo [10,17] nanostructures. The use of chromium in such studies has not gathered great interest, probably due to hexavalent chromium being extremely toxic and its trivalent chromium 'green' alternative having rather complex electrochemistry.

Electrodeposition of FeCrNi stainless steel-like coatings from a 'green' Cr(III) electrolyte has been shown to have outstanding characteristics: high corrosion resistance, low cytotoxicity and soft-magnetic properties [20]. The combination of electrodeposition and AAO nanotemplates for creating FeCrNi NWs can revolutionise the future progress in bio-medicine and micro-robotics. However, the use of Cr(III) for obtaining chromium-based nanostructures is limited [21–23]. Cr(III) chemistry

requires high applied potentials ($\text{Cr(III)} \rightarrow \text{Cr(0)}$, $E_0 = -0.72$ V vs. SHE) for the reduction of chromium ions to metallic chromium. Consequently, the HER is enhanced and leads to low deposition efficiencies [24–26]. This is the limiting factor for growing thick FeCrNi films without stresses and porosity issues, making it challenging to deposit into high AR moulds. Improving Cr(III)-based aqueous electrodeposition has been possible by using a complexing agent [24,27–29], as well as studying and understanding the various mechanisms involved in the electrochemical system, as reported in our previous study [30]. Another method for decreasing or avoiding these problems is using ionic liquids. The use of molten salts (with or without water) makes it possible to obtain films with higher deposition efficiencies and avoid concurrent HER [31–34]. However, these solutions are expensive, requiring the use of a glove-box and they are not always compatible with standard photoresists and other polymers used for micro-templating.

The aim of this work is to investigate an alternative pathway to electrodeposit FeCrNi NWs by employing a 'green' Cr(III)-based electrolyte. For this reason, a mixed-solvent solution comprised of EG has been found to be the most suitable and it has been used to decrease the impact of HER during cathodic electroreduction processes. For the first time, the electrodeposition of FeCrNi nanostructures from both a mixed-solvent and an aqueous solution into AAO membranes is reported. In case of the mixed 30 vol% EG electrolyte, either NWs or NTs can be grown depending on the applied current density. The outcome of this study is then compared to pre-existing kinetic models of metal ions deposited into nanotemplates and a possible explanation concerning the growth mechanisms occurring during FeCrNi ternary alloy electrodeposition inside nanoporous AAO templates is given.

2. Material and methods

2.1. Fabrication of FeCrNi films and nanostructures

FeCrNi films, NWs, and NTs were deposited using a standard three electrode electrochemical cell equipped with a water double jacket for temperature control (see schematic of the electrodeposition framework in Fig. 1).

The temperature of the electroplating bath was set to $22 \text{ }^\circ\text{C} \pm 0.5 \text{ }^\circ\text{C}$ using a temperature controlled circulator (Julabo, F12-ED). The electrochemical cell was comprised of a saturated Ag/AgCl electrode as the reference electrode, a platinum mesh (80 meshes, $25 \text{ mm} \times 35 \text{ mm}$, ALS Co., Ltd) as the counter electrode and depending on films or nanostructures the working electrode was different. For films, a flat substrate was

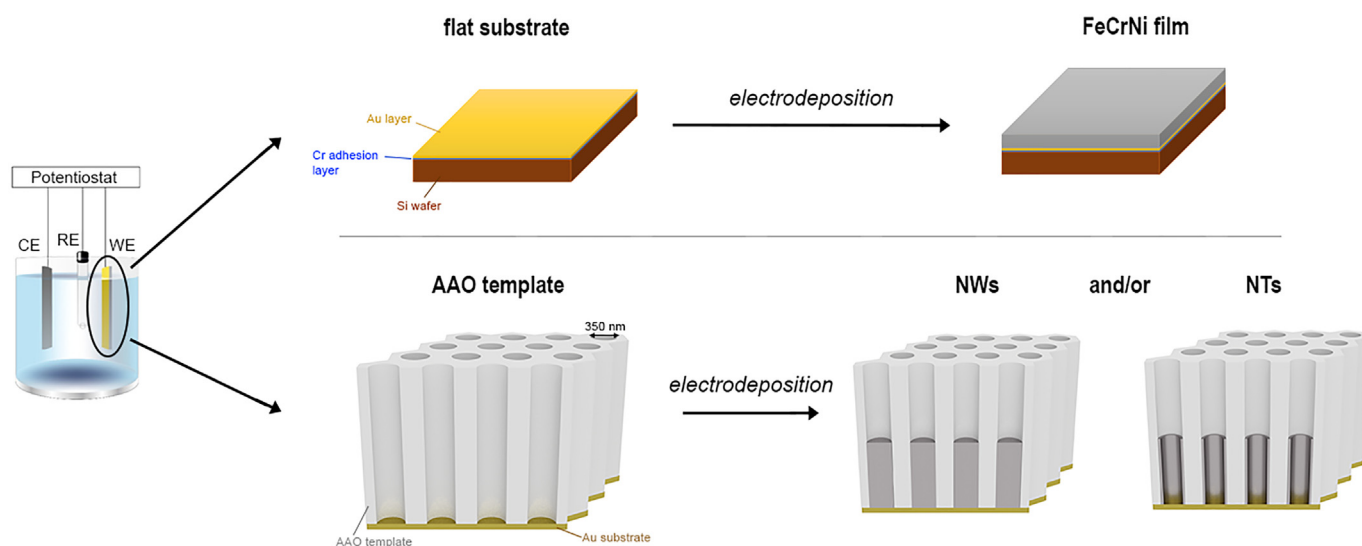


Fig. 1. Schematic of the electrodeposition protocol used for obtaining FeCrNi coatings (using a flat substrate) and nanostructures (using nanoporous AAO templates sputtered with Cr and Au).

used (100 nm Au/5 nm Cr/Si) as in the works of Hasegawa *et al.* [35] and Bertero *et al.* [20]. Commercial membranes (Smartmembranes GmbH, Germany) with 50 μm thickness and 350 nm diameter pores were sputtered with 5 nm Cr and 150 nm Au and were used as the substrate to obtain NWs and/or NTs. After electrodeposition, the AAO templates were dissolved via chemical etching in chromic oxide (1.8 wt%) and phosphoric acid (7 wt%, 85%) aqueous solution mixture at room temperature. The compositions of the various electrolytes used for FeCrNi electrodeposition are shown in Table 1.

Each electrolyte shares the same compounds and molar concentration, with only a difference in the solvent used. For the *Standard aqueous* electrolyte the solvent was only DI water as in our previous work [20,35]. For the 30 vol% EG and the 50 vol% EG electrolytes, the solvent was a mixture of DI water with addition of EG ($\geq 99\%$ purity) in proportion of 30 vol% and 50 vol% of the final total volume, respectively. The bath constituents were mixed similarly to the procedure described in our previous works [20,35]. The Cr(III) and glycine solution was first complexed in DI water at 80 °C for 30 min. After this, a second solution containing all other components was added and the solution was mixed. Finally, the volume was adjusted to reach 400 mL with either DI water or EG to reach the final desired volume proportions as shown in Table 1. All chemicals were of reagent grade (Sigma-Aldrich) and were used as-received without any further purification. Electrodeposition was carried out galvanostatically using a potentiostat (PGSTAT 302N, Metrohm Autolab B.V.) controlled by the NOVA (version 2.1) software. FeCrNi films were electrodeposited until a total charge of 400 C was reached. Different current densities were applied depending on the electrolyte to obtain similar compositions: -80 mA/cm^2 (average $E_{\text{dep}} -1.44\text{ V vs. Ag/AgCl}$), -50 mA/cm^2 (average $E_{\text{dep}} -1.52\text{ V vs. Ag/AgCl}$) and -30 mA/cm^2 (average $E_{\text{dep}} -1.65\text{ V vs. Ag/AgCl}$) corresponding to *Standard aqueous* solution, 30 vol% EG and 50 vol% EG mixed-solvent electrolytes, respectively.

2.2. Chemical, morphology and composition characterisations

Linear sweep voltammetry was performed for flat substrates using the previously mentioned set-up (standard three-electrode electrochemical cell and a potentiostat) with a scan rate (SR) equal to 10 mV/s and varying the potential from -0.25 to $-1.75\text{ V vs. Ag/AgCl}$, with a measured open circuit potential (OCP) of 0.40 V vs. Ag/AgCl.

UV–Vis absorbance spectra of freshly prepared FeCrNi electrolytes (*i.e.* *Standard aqueous*, 30 vol% EG, 50 vol% EG) were measured after diluting 10 times the original solution into the corresponding solvent (*i.e.* deionised water, 30 vol% EG, 50 vol% EG) using a UV–Vis spectrophotometer (UV–Vis PerkinElmer Lambda 900 UV, PerkinElmer) in the wavelength range between 350 and 700 nm in a 10 mL quartz cell. Prior each measurement, for each electrolyte, the corresponding solvent baseline has been taken into account by the software via background subtraction.

Table 1

Composition of the various FeCrNi electrolytes.

| | Standard aqueous electrolyte | 30 vol% EG electrolyte | 50 vol% EG electrolyte |
|---|------------------------------|------------------------|------------------------|
| | Concentration (mol/L) | | |
| $\text{CrCl}_3 \cdot 6\text{H}_2\text{O}$ | 0.4 | 0.4 | 0.4 |
| Glycine ($\text{NH}_2\text{CH}_2\text{COOH}$) | 0.4 | 0.4 | 0.4 |
| $\text{FeCl}_2 \cdot 4\text{H}_2\text{O}$ | 0.03 | 0.03 | 0.03 |
| $\text{NiCl}_2 \cdot 6\text{H}_2\text{O}$ | 0.2 | 0.2 | 0.2 |
| NH_4Cl | 0.5 | 0.5 | 0.5 |
| H_3BO_3 | 0.15 | 0.15 | 0.15 |
| NaCl | 0.5 | 0.5 | 0.5 |
| Water volume (mL) | 400 | 300 | 220 |
| EG volume (mL) | – | 100 | 180 |
| Total volume (mL) | 400 | 400 | 400 |

pH: 1, Temperature: 22 °C.

The surface morphology of the FeCrNi coatings was observed via field-emission scanning electron microscopy (FE-SEM, Hitachi S-4800, Hitachi High-Technologies Corporation).

X-ray fluorescence (XRF, Fischerscope® X-RAY XDV®-SDD, Fischer Technology) was used to estimate the Fe–Cr–Ni wt% and thicknesses along the film's area. The measurements were performed at 25 uniformly distributed points on each specimen and the average of the 9-matrix central points was chosen as the representative concentration. Approximate current efficiencies (C.E., %) from XRF thickness measurements were calculated by knowing the weight percentage of each metal element, assuming the density of stainless steel to be $\rho_{\text{SS}} = 7.93\text{ g/cm}^3$ and using Faraday's law.

The elemental composition (in at%) of the metal species (Fe, Cr and Ni) and impurities (O, C and N) was evaluated via X-ray photoelectron spectroscopy (XPS) on the coatings' surface and profiling at different depths from the surface down to approximately 500 nm. This was achieved by sputtering the material with Ar^+ ions (2 or 4 keV sputtering energy). The representative concentrations were the ones measured after approximately 50 min of sputtering time in-depth of the coating, with the standard deviation calculated taking into account various depth concentrations around the representative one. XPS data was acquired using a Physical Electronics (PHI) Quantum 2000 Scanning ESCA Microprobe System composed by a monochromatic Al K α X-ray radiation source ($h\nu = 1486.7\text{ eV}$) of 29.7 W power with a typical beam diameter of 150 μm and a hemispherical capacitor electron-energy analyser equipped with a channel plate and a position-sensitive detector. Electron take-off angle was of 45 ° and the analyser operated in the constant pass energy mode at 29.35 eV. Compensation of eventual surface charging was performed with built-in electron and argon ion neutralizers. The base pressure of the system was below $5 \times 10^{-7}\text{ Pa}$ and the binding energy was calibrated using Cu 2p $_{3/2}$, Ag 3d $_{5/2}$ and Au 4f $_{7/2}$ at 932.62 eV, 368.21 eV and 83.96 eV, respectively to within $\pm 0.1\text{ eV}$. The spectra was analysed by means of CasaXPS software [36] (version 2.3.19).

Additionally, the H ratio in at% with respect to all metal species (Fe, Cr and Ni) was determined in-depth up to 200 nm by helium elastic recoil detection analysis (He-ERDA, ETH Zurich) using a 2 MeV He beam and the absorber foil technique [37]. The representative concentration of hydrogen was the one measured after approximately 20 min sputtering time in-depth of the coating, with the standard deviation calculated by taking into account various depth concentrations around the representative one.

The morphology characterisation of the NWs/NTs from AAO template cross-section images was performed using two SEM set-up: Hitachi (FE-SEM, Hitachi S-4800, Hitachi High-Technologies Corporation) with a 1.5 kV accelerating voltage and Lyra (dual-beam FE-SEM/Ga FIB, Tescan Lyra3, Tescan Orsay holding a.s.) with a 15 kV accelerating voltage. Compositional characterisation (Fe–Cr–Ni–O–C, at%) of the dissolved NWs was carried out by energy dispersive X-ray (EDX) analysis on the Lyra system with a 30 kV accelerating voltage.

3. Results and discussion

3.1. UV–Vis absorption spectra of FeCrNi aqueous and mixed-solvent electrolytes

The UV–Vis absorption measurements were performed for freshly prepared FeCrNi electrolytes with different concentration of solvents and their spectra were compared (Fig. 2). All electrolytes show peaks at $\lambda_1 = 580\text{ nm}$ and $\lambda_2 = 410\text{ nm}$, indicating Cr(III) is complexed with glycine as shown previously [30,38,39].

Complexation of chromium to glycine is essential for promoting Cr (III) electroreduction at the cathode, otherwise Cr(III)-aqua complexes would be favoured and no deposition achieved. In this case, the use of EG in the FeCrNi electrolyte does not influence Cr(III)-glycine complexation (identical peaks position), showing that EG-based electrolytes are also favourable for deposition. Increasing the amount of EG in the

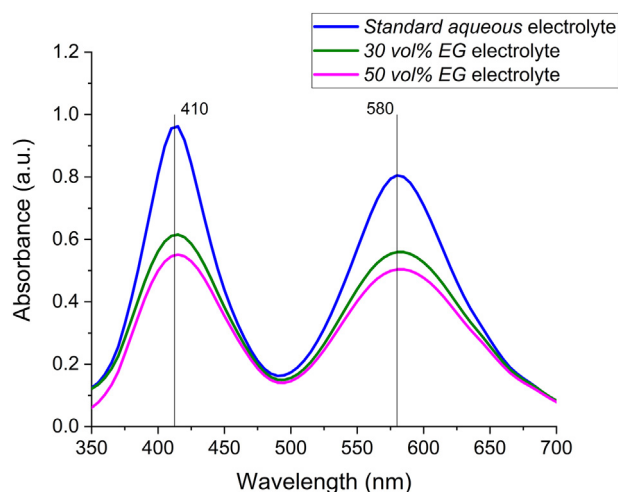


Fig. 2. UV-Vis spectra of various freshly prepared FeCrNi electrolytes diluted 10 times in the corresponding solvent.

electrolyte from 0 vol% (*Standard aqueous* electrolyte) to 30 vol% (30 vol% EG electrolyte) to 50 vol% (50 vol% EG electrolyte), the absorption intensity is decreasing. This is because EG is affecting Cr(III)-glycine surroundings, making it more difficult for such complexes to absorb light, with a consequent decrease in the peaks intensity when EG volume in the electrolyte is increased.

3.2. FeCrNi films electrodeposited from aqueous and mixed-solvent electrolytes

3.2.1. Linear sweep voltammetry (LSV)

LSV have been used to retrieve the reduction potentials for the elements involved in the electrodeposition process (i.e. Fe, Cr, Ni) among the different analysed electrolytes. From Fig. 3, it can be seen that both

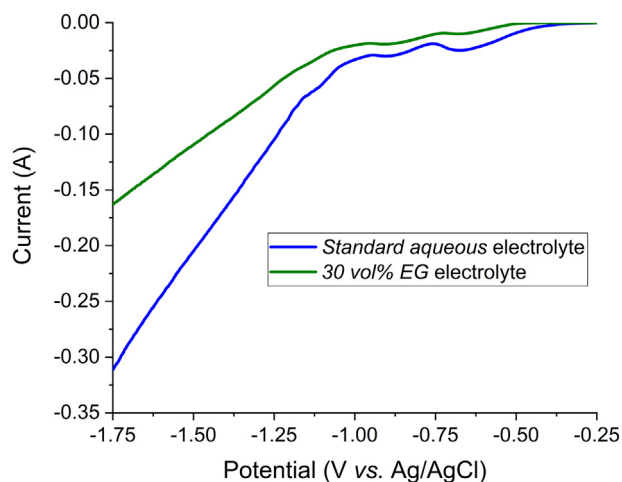


Fig. 3. LSV potentiostats on flat Au substrates from FeCrNi electrolytes: *Standard aqueous* and mixed-solvent 30 vol% EG.

FeCrNi *Standard aqueous* and 30 vol% EG mixed-solvent solutions have similar reduction peak positions: at -0.67 V vs. Ag/AgCl corresponding to Ni(II) to Ni(0) ($E^0 = -0.25$ V vs. SHE), at -0.89 V vs. Ag/AgCl corresponding to Fe(II) to Fe(0) ($E^0 = -0.44$ V vs. SHE) and at -1.14 V vs. Ag/AgCl corresponding most likely to the first reduction step of complexed chromium (Cr(III)-glycine) from Cr(III) to Cr(II) ($E^0 = -0.42$ V vs. SHE). The second reduction potential of chromium is probably hidden by the higher current consuming concurrent HER.

From these LSV results, it is noticeable that for the same applied potential (i.e. FeCrNi $E_{\text{dep}} \approx -1.5$ V vs. Ag/AgCl), the corresponding current is lower for the mixed-solvent case with respect to the aqueous FeCrNi electrolyte counterpart. This already provides evidence that for the mixed-solvent solution, the HER is less active.

3.2.2. Elemental composition and deposition efficiency

The composition in wt% and the current efficiencies (C.E.) of the electrodeposited FeCrNi films has been estimated by means of XRF technique. For the *Standard aqueous* solution the coating is $\text{Fe}57.0 \pm 1.6$ - $\text{Cr}28.3 \pm 1.7$ - $\text{Ni}14.7 \pm 0.8$ wt% (C.E. 6.2%), whereas for the 30 vol% EG and 50 vol% EG electrolytes are $\text{Fe}54.0 \pm 2.9$ - $\text{Cr}29.1 \pm 3.2$ - $\text{Ni}16.8 \pm 0.5$ wt% (C.E. 9.1%) and $\text{Fe}56.4 \pm 1.4$ - $\text{Cr}26.6 \pm 1.8$ - $\text{Ni}17.0 \pm 1.0$ wt% (C.E. 9.6%), respectively. The elemental contents measured in-depth in at% of Fe-Cr-Ni-O-C-N (XPS, 50 min sputtering time) and H/metals ratio (He ERDA, 20 min sputtering time) were evaluated for the coatings obtained by using two different EG mixed-solvent electrolytes (i.e. 30 vol% EG and 50 vol% EG) and compared with the results for a film deposited using a *Standard aqueous* solution [30] (Table 2).

Based on these results, it seems that the decrease in water content (due to EG) inside the electrolyte is positively affecting the current efficiency, which increases in both EG cases by approx. 1.5 times with respect to the aqueous counterpart. Regarding the incorporation of impurities (i.e. O, C, N and H), the hydrogen content is similar among all produced coatings, regardless of the used electrolyte. The only noticeable difference among aqueous and mixed-solvent electrolytes is the carbon content, which is half the all-aqueous value when using the EG solutions. These outcomes can be explained by looking at the FeCrNi electroreduction mechanisms proposed in our previous work for aqueous electrolyte [30]. The lower fraction of water in solution reduces the influence of HER at the cathode and, thus, most probably, decreases the incorporation of unwanted carboxyl groups from Cr(III)-glycine hydroxides/hydrides adsorbed molecules, mainly reducing the concentration of carbon within the coating. This fact should also have a positive effect on the mechanical properties of the material, e.g. by lowering the electrodeposit's brittleness. The ductility of stainless steel alloys is typically linked to the amount of incorporated carbon [40].

3.3. FeCrNi nanostructures electrodeposited from aqueous and mixed-solvent electrolytes

3.3.1. Morphology and elemental composition

Electrodeposition into AAO templates from *Standard aqueous* solution at different current densities led to either completely empty channels or hardly any deposited material. SEM cross-section images of a sample obtained by electrodepositing at -20 mA/cm² (Fig. 4) show that this is the only case where sporadic compact material was observed, with the rest of the template remaining unfilled.

Table 2
Elemental composition in-depth of Fe-Cr-Ni-O-C-N (XPS, 50 min sputtering time) and of H (He-ERDA, 20 min sputtering time) of electrodeposited FeCrNi films produced from *Standard aqueous* [30], 30 vol% EG and 50 vol% EG mixed-solvent electrolytes.

| Electrolyte | Fe (at%) | Cr (at%) | Ni (at%) | O (at%) | C (at%) | N (at%) | H (at%)/metals |
|-------------------------|----------------|----------------|----------------|----------------|----------------|---------------|----------------|
| <i>Standard aqueous</i> | 37.8 ± 0.2 | 15.8 ± 0.1 | 11.7 ± 0.1 | 16.8 ± 0.0 | 16.4 ± 0.0 | 1.5 ± 0.1 | 16.0 ± 1.7 |
| 30 vol% EG | 44.1 ± 0.2 | 15.4 ± 0.4 | 15.8 ± 0.1 | 15.8 ± 0.1 | 7.6 ± 0.0 | 1.3 ± 0.0 | 15.0 ± 1.3 |
| 50 vol% EG | 41.4 ± 0.3 | 16.0 ± 0.1 | 16.5 ± 0.2 | 17.5 ± 0.3 | 7.4 ± 0.2 | 1.1 ± 0.0 | 17.5 ± 1.7 |

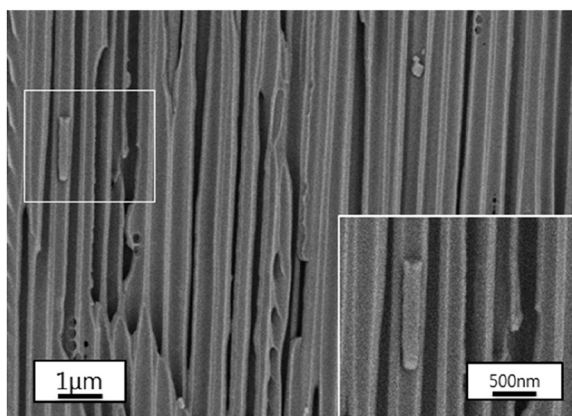


Fig. 4. SEM cross-section images of electrodeposited FeCrNi into AAO template from Standard aqueous electrolyte.

In contrast, the electrodeposition of FeCrNi from the mixed-solvent 30 vol% EG electrolyte shows all samples exhibiting a higher filling ratio than the aqueous solution cases, i.e. from $<10\ \mu\text{m}$ applying a relatively low current density ($-5\ \text{mA}/\text{cm}^2$), up to $30\ \mu\text{m}$ when doubling

the current density ($-10\ \text{mA}/\text{cm}^2$). At a high current density the pore filling followed a cylindrical growth with the formation of NTs, as shown in the SEM cross-section images (Fig. 5a1, a2, a3, a4). At a low current density the material is more compact, resulting in NWs (Fig. 5b1, b2, b3).

When dissolving the AAO template for the various studied electrodeposited samples, it was possible to recover only a few NWs from the low current density case (Fig. 5b4, b5). The atomic compositions of such NWs have been measured by using the EDX technique. The presence of carbon in the spectra is caused by the carbon matrix background, and other impurities (i.e. oxygen and nitrogen) are not considered in this discussion due to the measurement uncertainty for these elements. The NWs are mainly formed by Fe, Cr and Ni. The atomic contents of these three elements along a single NW are rather homogeneous (Table 3). However, for different NWs of the same analysed sample, Fe-Cr-Ni contents vary. This could be due to an uneven primary current distribution (PCD) present in different parts of the samples (i.e. center and edges) during electrodeposition.

3.3.2. Kinetic and growth model correlation

The possible mechanisms explaining the behaviour of this ternary FeCrNi electrochemical system are schematically drawn in Fig. 6. When a relative high current density is applied, the HER forms H_2

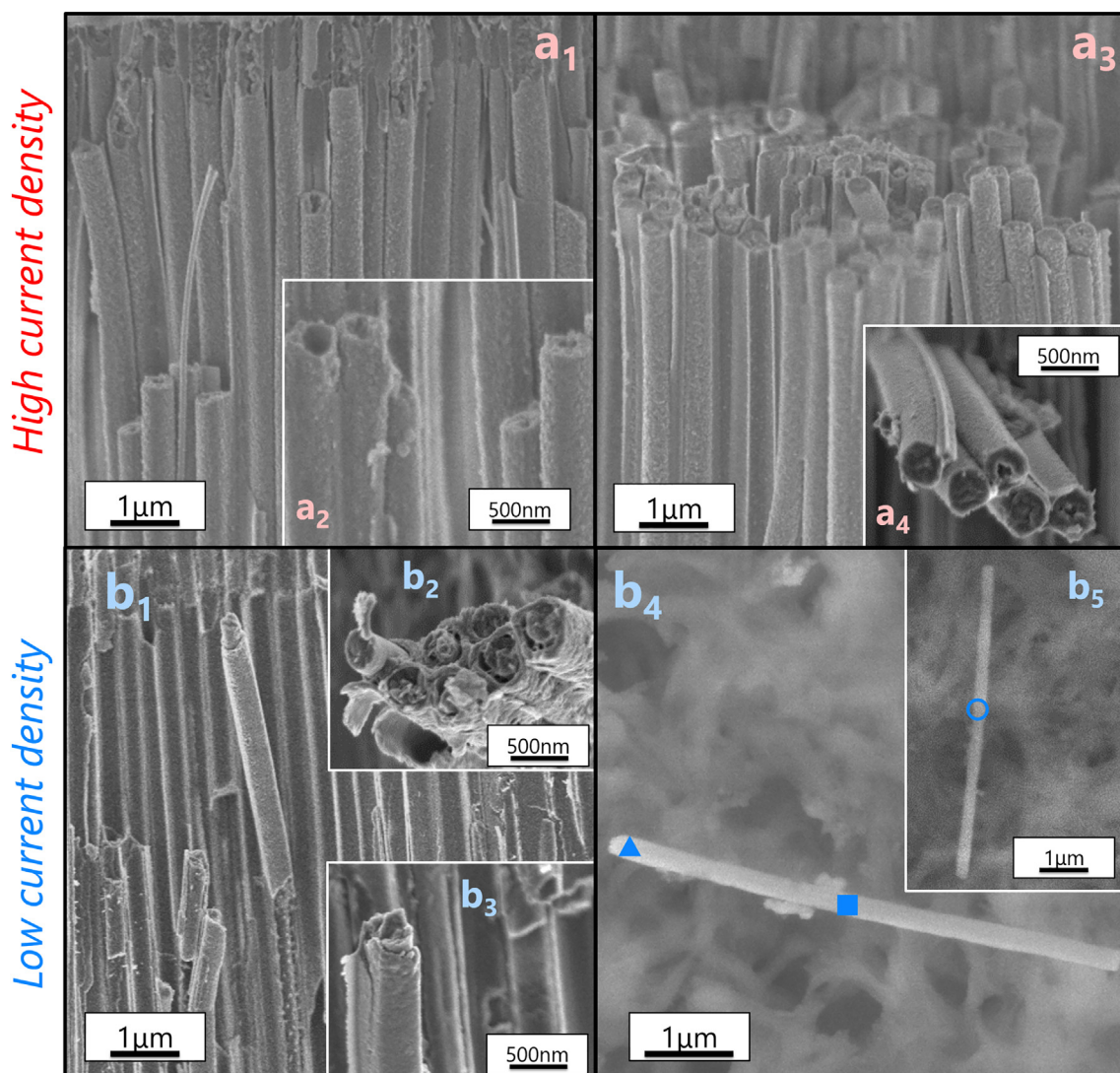


Fig. 5. SEM cross-section images of electrodeposited FeCrNi inside AAO templates from mixed-solvent 30 vol% EG: (a1, a2, a3, a4) at a higher current density ($-10\ \text{mA}/\text{cm}^2$) nanotube growth, (b1, b2, b3) at a lower current density ($-5\ \text{mA}/\text{cm}^2$) nanowire growth. (b4, b5) SEM top-view images of dissolved single FeCrNi NWs.

Table 3

Elemental composition of Fe–Cr–Ni (EDX) in at% at different points of single electrodeposited FeCrNi NWs (from Fig. 5).

| | Fe (at%) | Cr (at%) | Ni (at%) |
|----------|----------|----------|----------|
| Triangle | 64.3 | 4.9 | 30.8 |
| Square | 66.9 | 3.1 | 30.0 |
| Ring | 53.6 | 26.1 | 20.3 |

bubbles that escape from the pores. The combination of more intense PCD at the edges of the pores and a favourable pathway for H₂ bubbles at the center of each AAO pore force the material to mainly grow on the side-walls, leading to the formation of nanotubes, which are longer and less compact. However, when a relatively low current density is used, HER is less pronounced, as well as PCD. Consequently, the growth inside the pores is more homogenous, producing shorter, but denser NWs. This work's experimental results and the proposed mechanisms can be correlated with the kinetic model explained by Philippe *et al.* [18,19] for the electrodeposition of Co into high aspect ratio nanoelectrodes. In that study, the growth inside nanoporous templates was linked to two main factors. First, metal ions follow a spherical diffusion-controlled regime when steady state is reached (*i.e.* Nernst diffusion layer becomes larger than the template thickness) and, second, the occurrence of pH variation inside the pores due to the HER. We propose that this model is also valid for more complex electrochemical systems such as the FeCrNi ternary system.

4. Conclusions

The electrodeposition of a stainless steel-like FeCrNi ternary alloy was investigated both in aqueous and mixed-solvent EG electrolytes

on flat substrates and inside nanoporous anodic alumina templates. EG-based baths required lower current densities at the same deposition potentials, when compared to their aqueous counterpart, showing that the parasitic HER consumed less current during electrodeposition. The comparison of metal contents and impurities in-depth of the studied coatings revealed identical compositions, except for carbon at%, which was reduced by half in the case of the mixed-solvent electrolyte. The decrease in both HER and carbon content can be beneficial factors for improving electrodeposition into miniaturised moulds by increasing current efficiency and thus mechanical properties of the material.

Electrodepositing into AAO templates from an aqueous FeCrNi electrolyte resulted in almost no filling of the pores. By using a 30 vol% EG mixed-solvent it was possible to grow up to 30 µm thick material inside the templates. The main parameter affecting the deposition inside the nanoscale pores was the current density. Depending on current density, NWs or NTs could be grown inside the moulds. EDX measurements of Fe–Cr–Ni contents of the dispersed NWs showed that the composition was homogenous along the nanowire length, but dissimilar when analysing different NWs for the same sample.

For the first time, it is revealed that FeCrNi nanostructures can be achieved *via* electroplating into AAO templates from a Cr(III)-based mixed-solvent electrolyte. Moreover, the shape of such nanostructures can be controlled by varying the current density, fabricating either NTs or NWs using higher or lower currents, respectively. Such a phenomenon can be explained by the kinetic and growth models present in the literature for single metals electrodeposited into nano-moulds. These preliminary results are promising in terms of the feasibility of producing FeCrNi micro- and nanocomponents by means of the presented deposition method. Furthermore, FeCrNi NWs and NTs can pave the way for future applications in the fields of micro-robotics and bio-medicine.

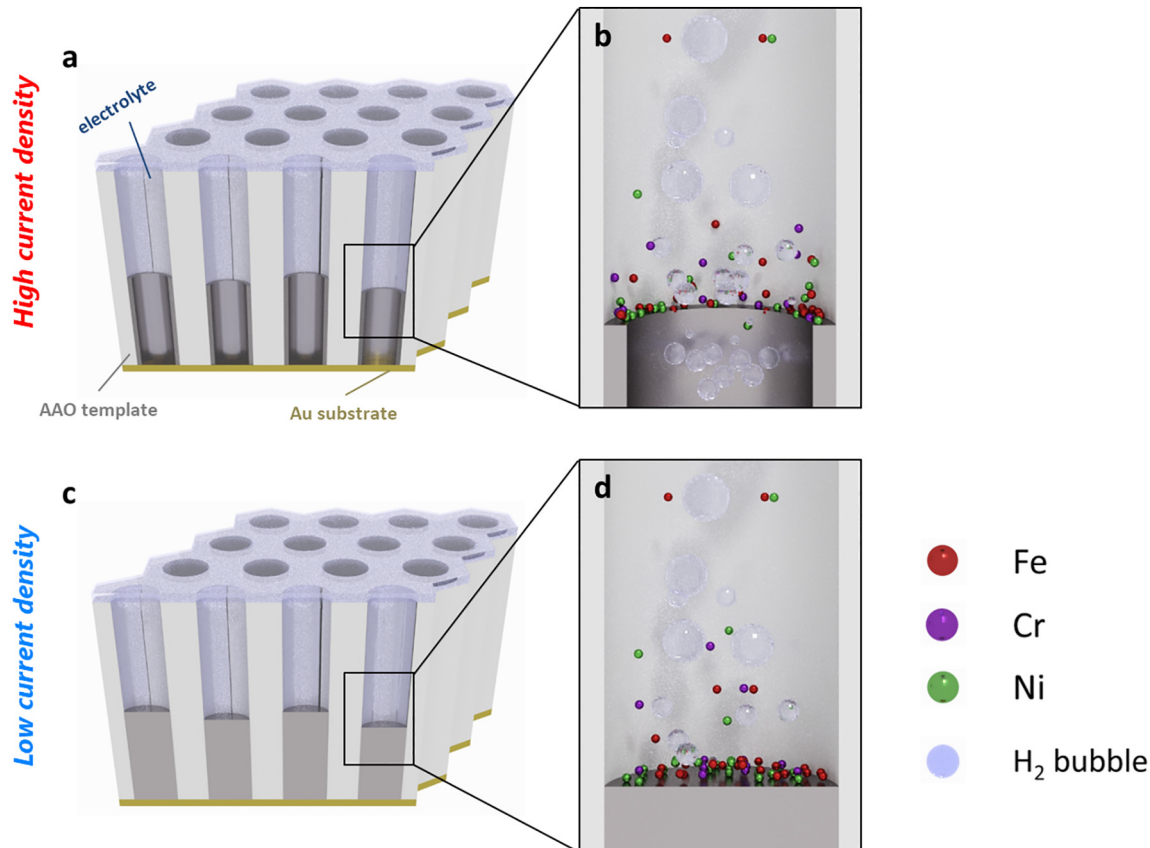


Fig. 6. Schematic of the possible growth mechanisms proceeding inside AAO templates during the electrodeposition of FeCrNi: (a, b) NTs produced at a higher current density, (c, d) NWs created at a lower current density.

Data availability

The raw/processed data required to reproduce these findings cannot be shared at this time due to technical or time limitations.

CRediT authorship contribution statement

Enrico Bertero: Conceptualization, Methodology, Formal analysis, Investigation, Data curation, Writing - original draft, Writing - review & editing, Visualization. **Cristina V. Manzano:** Conceptualization, Investigation, Writing - original draft, Writing - review & editing. **Gerhard Bürki:** Investigation. **Laetitia Philippe:** Conceptualization, Methodology, Writing - original draft, Writing - review & editing, Supervision, Project administration.

Declaration of competing interest

The authors declare that they have no known competing financial interests or personal relationships that could have appeared to influence the work reported in this paper.

Acknowledgements

This work was partially supported by the European project SELECTA-ETN (H2020-MSCA-ITN-2014 no. 642642) and the e-MINDS COST Action (no. MP1407) from the EU Horizon 2020 Framework Programme. The authors thank *Laboratory for Nanoscale Materials Science - Empa Dübendorf* for the XPS measurements and Dr. Max Döbeli (doebeli@phys.ethz.ch) from *Laboratory for Ion Beam Physics - ETH Zürich* for ERDA characterisation. Additionally, we are grateful to Laszlo Pethö (laszlo.petho@empa.ch) of *Empa Thun* for Au sputtering process, Patrik Schürch (patrik.schuerch@empa.ch) of *Empa Thun* for helping with the rendering images, both Caroline Hain (caroline.hain@empa.ch) and Dr. Christopher Gunderson (christopher.gunderson@empa.ch) of *Empa Thun* for English corrections.

References

- [1] D. Clark, D. Wood, U. Erb, Industrial applications of electrodeposited nanocrystals, *Nanostructured Mater* 9 (1997) 755–758, [https://doi.org/10.1016/S0965-9773\(97\)00163-3](https://doi.org/10.1016/S0965-9773(97)00163-3).
- [2] M. Niinomi, *Metals for Biomedical Devices*, CRC Press, 2010.
- [3] S. Bhansali, A. Vasudev, MEMS for biomedical applications, *MEMS Biomed. Appl. InTech* 2012, pp. 1–487, <https://doi.org/10.1533/9780857096272>.
- [4] T. Osaka, M. Datta, Y. Shacham-Diamand, *Electrochemical Nanotechnologies*, Springer Science & Business Media, 2009.
- [5] J. Martín, C.V. Manzano, M. Martín-González, In-depth study of self-ordered porous alumina in the 140–400 nm pore diameter range, *Microporous Mesoporous Mater.* 151 (2012) 311–316, <https://doi.org/10.1016/j.micromeso.2011.10.018>.
- [6] J. Martín, C.V. Manzano, O. Caballero-Calero, M. Martín-González, High-aspect-ratio and highly ordered 15-nm porous alumina templates, *ACS Appl. Mater. Interfaces* 5 (2013) 72–79, <https://doi.org/10.1021/am3020718>.
- [7] C.V. Manzano, J. Martín, M.S. Martín-González, Ultra-narrow 12 nm pore diameter self-ordered anodic alumina templates, *Microporous Mesoporous Mater.* 184 (2014) 177–183, <https://doi.org/10.1016/j.micromeso.2013.10.004>.
- [8] C.V. Manzano, J.P. Best, J.J. Schwedrzik, A. Cantarero, J. Michler, L. Philippe, The influence of thickness, interpore distance and compositional structure on the optical properties of self-ordered anodic aluminum oxide films, *J. Mater. Chem. C* 4 (2016) 7658–7666, <https://doi.org/10.1039/C6TC01904H>.
- [9] C.V. Manzano, G. Bürki, L. Pethö, J. Michler, L. Philippe, Determining the diffusion mechanism for high aspect ratio ZnO nanowires electrodeposited into anodic aluminum oxide, *J. Mater. Chem. C* 5 (2017) 1706–1713, <https://doi.org/10.1039/C6TC04921D>.
- [10] A. Saeidi, M. Ghorbani, Electrodeposition of Ni–Fe–Co alloy nanowire in modified AAO template, *Mater. Chem. Phys.* 91 (2005) 417–423, <https://doi.org/10.1016/j.materchemphys.2004.12.001>.
- [11] H. Pan, B. Liu, J. Yi, C. Poh, S. Lim, J. Ding, Y. Feng, C.H.A. Huan, J. Lin, Growth of single-crystalline Ni and Co nanowires via electrochemical deposition and their magnetic properties, *J. Phys. Chem. B* 109 (2005) 3094–3098, <https://doi.org/10.1021/jp0451997>.
- [12] J. Qin, J. Nogués, M. Mikhaylova, A. Roig, J.S. Muñoz, M. Muhammed, Differences in the magnetic properties of Co, Fe, and Ni 250–300 nm wide nanowires electrodeposited in amorphous anodized alumina templates, *Chem. Mater.* 17 (2005) 1829–1834, <https://doi.org/10.1021/cm047870q>.
- [13] W.O. Rosa, L.G. Vivas, K.R. Pirotta, A. Asenjo, M. Vázquez, Influence of aspect ratio and anisotropy distribution in ordered CoNi nanowire arrays, *J. Magn. Mater.* 324 (2012) 3679–3682, <https://doi.org/10.1016/j.jmmm.2012.05.047>.
- [14] G.J. Strijkers, J.H.J. Dalderop, M.A.A. Broeksteeg, H.J.M. Swagten, W.J.M. de Jonge, Structure and magnetization of arrays of electrodeposited Co wires in anodic alumina, *J. Appl. Phys.* 86 (1999) 5141–5145, <https://doi.org/10.1063/1.371490>.
- [15] S. Thongmee, H.L. Pang, J. Ding, J.B. Yi, J.Y. Lin, Fabrication and magnetic properties of metal nanowires via AAO templates, 2008 2nd IEEE Int. Nanoelectron. Conf., IEEE 2008, pp. 1116–1120, <https://doi.org/10.1109/INEC.2008.4585678>.
- [16] I. Dobosz, W. Gumowska, M. Czapkiewicz, Magnetic properties of Co-Fe nanowires electrodeposited in pores of alumina membrane, *Arch. Metall. Mater.* 58 (2013) 663–671, <https://doi.org/10.2478/amm-2013-0052>.
- [17] D. Li, E. Podlaha, Template-assisted electrodeposition of Fe–Ni–Co nanowires: effects of electrolyte pH and sodium lauryl sulfate, *J. Electrochem. Soc.* 164 (2017) D843–D851, <https://doi.org/10.1149/2.0931713jes>.
- [18] L. Philippe, J. Michler, A kinetic model enabling controlled electrosynthesis of stacked metallic nanotubes and nanowires, *Small* 4 (2008) 904–907, <https://doi.org/10.1002/smll.200800103>.
- [19] L. Philippe, N. Kacem, J. Michler, Electrochemical deposition of metals inside high aspect ratio nanoelectrode array: analytical current expression and multidimensional kinetic model for cobalt nanostructure synthesis, *J. Phys. Chem. C* 111 (2007) 5229–5235, <https://doi.org/10.1021/jp0677997>.
- [20] E. Bertero, M. Hasegawa, S. Staubli, E. Pellicer, I.K. Hermann, J. Sort, S. Mischler, J. Michler, L. Philippe, Electrodeposition of amorphous Fe–Cr–Ni stainless steel alloy with high corrosion resistance, low cytotoxicity and soft magnetic properties, *Surf. Coat. Technol.* 349 (2018) 745–751, <https://doi.org/10.1016/j.surfcoat.2018.06.003>.
- [21] N.B. Chauré, J.M.D. Coey, Fabrication and characterization of electrodeposited Co1–xCrx nanowires, *J. Magn. Mater.* 303 (2006) 232–236, <https://doi.org/10.1016/j.jmmm.2005.11.012>.
- [22] K. Maleki, Z. Alemipour, Electrodeposition and characterization of NiCr alloy nanowires, *Appl. Phys. A Mater. Sci. Process.* 123 (2017) 397, <https://doi.org/10.1007/s00339-017-1009-z>.
- [23] M. Najafi, Z. Alemipour, I. Hasanadeh, A. Aftabi, S. Soltanian, Influence of annealing temperature, electrolyte concentration and electrodeposition conditions on magnetic properties of electrodeposited Co–Cr alloy nanowires, *J. Supercond. Nov. Magn.* 28 (2015) 95–101, <https://doi.org/10.1007/s10948-014-2803-x>.
- [24] Y.B. Song, D.-T. Chin, Current efficiency and polarization behavior of trivalent chromium electrodeposition process, *Electrochim. Acta* 48 (2002) 349–356.
- [25] M. El-Sharif, J. McDougall, C.U. Chisholm, Electrodeposition of thick chromium coatings from an environmentally acceptable chromium (III)–glycine complex, *Trans. Inst. Met. Finish.* 77 (n.d.) 139–144, (<http://cat.inist.fr/?aMode=affiche&N&csid=1881722> (accessed June 23, 2016)).
- [26] S. Surviliene, O. Nivinskiene, A. Česūniene, A. Selskis, Effect of Cr(III) solution chemistry on electrodeposition of chromium, *J. Appl. Electrochem.* 36 (2006) 649–654, <https://doi.org/10.1007/s10800-005-9105-8>.
- [27] V. Protsenko, F. Danilov, Kinetics and mechanism of chromium electrodeposition from formate and oxalate solutions of Cr (III) compounds, *Electrochim. Acta* 54 (2009) 5666–5672.
- [28] J. McDougall, M. El-Sharif, S. Ma, Chromium electrodeposition using a chromium (III) glycine complex, *J. Appl. Electrochem.* 28 (1998) 929–934.
- [29] A. Baral, R. Engelken, Modeling, optimization, and comparative analysis of trivalent chromium electrodeposition from aqueous glycine and formic acid baths, *J. Electrochem. Soc.* 152 (2005) C504–C512.
- [30] E. Bertero, C.V. Manzano, E. Pellicer, J. Sort, R.M. Ullig, S. Mischler, J. Michler, L. Philippe, ‘Green’ Cr(III)–glycine electrolyte for the production of FeCrNi coatings: electrodeposition mechanisms and role of by-products in terms of coating composition and microstructure, *RSC Adv.* 9 (2019) 25762–25775, <https://doi.org/10.1039/C9RA04262H>.
- [31] V. Protsenko, L. Bobrova, F. Danilov, Trivalent chromium electrodeposition using a deep eutectic solvent, *Anti-Corrosion Methods Mater* 65 (2018) 499–505, <https://doi.org/10.1108/ACMM-05-2018-1946>.
- [32] G. Panzeri, M. Tresoldi, L. Nobili, L. Magagnin, Electrodeposition of ZnNi alloys from ethylene glycol/choline chloride based ionic liquid, *ECS Trans.* 75 (2016) 627–632, <https://doi.org/10.1149/07515.0627ecst>.
- [33] A.R. Kim, R.G. Reddy, Cobalt Electrodeposition From Cobalt Chloride Using Urea and Choline Chloride Ionic Liquid: Effect of Temperature, Applied Voltage, and Cobalt Chloride Concentration on Current Efficiency and Energy Consumption, *Springer, Cham*, 2017 97–114, https://doi.org/10.1007/978-3-319-51091-0_9.
- [34] A.P. Abbott, A.A. Al-Barzinjy, P.D. Abbott, G. Frisch, R.C. Harris, J. Hartley, K.S. Ryder, Speciation, physical and electrolytic properties of eutectic mixtures based on CrCl₃·6H₂O and urea, *Phys. Chem. Chem. Phys.* 16 (2014) 9047, <https://doi.org/10.1039/c4cp00057a>.
- [35] M. Hasegawa, S. Yoon, G. Guillonéau, Y. Zhang, C. Frantz, C. Niederberger, A. Weidenkaff, J. Michler, L. Philippe, The electrodeposition of FeCrNi stainless steel: microstructural changes induced by anode reactions, *Phys. Chem. Chem. Phys.* 16 (2014) 26375–26384, <https://doi.org/10.1039/c4cp03744h>.
- [36] N. Fairley, CasaXPS: Spectrum Processing Software for XPS, AES and SIMS, ©CasaXPS Ltd, 2005. <http://www.casaxps.com/>.
- [37] M. Nastasi, J.W. Mayer, Y. Wang, *Ion Beam Analysis: Fundamentals and Applications*, CRC Press, 2014.
- [38] S. Surviliene, A. Česūniene, A. Selskis, R. Butkienė, Effect of Cr(III)–Ni(II) solution chemistry on electrodeposition of CrNi alloys from aqueous oxalate and glycine baths, *Trans. IMF.* 91 (2013) 24–31, <https://doi.org/10.1179/0020296712Z.0000000060>.
- [39] B. Li, A. Lin, X. Wu, Y. Zhang, F. Gan, Electrodeposition and characterization of Fe–Cr–P amorphous alloys from trivalent chromium sulfate electrolyte, *J. Alloys Compd.* 453 (2008) 93–101, <https://doi.org/10.1016/j.jallcom.2006.11.162>.
- [40] G.E. Totten, M.A.H. Howes, *Steel Heat Treatment Handbook*, CRC Press, 1997.